Available online at www.sciencedirect.com

SCIENCE DIRECT®

Earth and Planetary Science Letters 223 (2004) 349–364

EPSL

www.elsevier.com/locate/epsl

$^{40}Ar-^{39}Ar$ dating of pseudotachylytes: the effect of clast-hosted extraneous argon in Cenozoic fault-generated friction melts from the West Antarctic Rift System☆

Gianfranco Di Vincenzo[a,*], Sergio Rocchi[b], Federico Rossetti[c], Fabrizio Storti[c]

[a] *Istituto di Geoscienze e Georisorse- CNR, via Moruzzi, 1, I-56124 Pisa, Italy*
[b] *Dipartimento di Scienze della Terra, Università di Pisa, via S. Maria 53, I-56126 Pisa, Italy*
[c] *Dipartimento di Scienze Geologiche, Università degli studi "Roma Tre", Largo S. Leonardo Murialdo 1, I-00146, Roma, Italy*

Received 22 January 2004; received in revised form 26 April 2004; accepted 29 April 2004

Abstract

Fault-generated pseudotachylytes are the product of frictional melting during high-velocity slip associated with coseismic faulting. $^{40}Ar-^{39}Ar$ dating of pseudotachylytes represents a powerful tool to directly determine the age of brittle faulting which is otherwise dated only indirectly. However, the pronounced spatial heterogeneity of most endogenically generated pseudotachylytes, due to the intimate coexistence of unmelted mineral clasts from the source rock, frictional glass and neogenic igneous minerals, often precludes a straightforward interpretation of argon data. This requires careful evaluation of the role of clasts in plaguing the age record of the pseudotachylyte matrix. This study exploits the full potential of the $^{40}Ar-^{39}Ar$ method, using laser step-heating and laser in situ techniques in conjunction with textural and chemical characterisation at the microscale to disentangle the complexity of the first record of pseudotachylytes generated in the right-lateral fault systems which dissect the western shoulder of the West Antarctic Rift System. Pseudotachylytes occur as fault and injection veins. They exhibit glassy matrices with a potassium feldspar-like composition, and invariably contain, at a millimeter to microscopic scale, unmelted quartz and subordinate feldspars from the source rock. Injection veins characteristically contain much fewer mineral clasts. In situ ultraviolet (UV) laser analyses indicate that quartz from the host rock and from clasts within the fault veins contains significant amounts ($\sim 10-50$ ppb) of parentless ^{40}Ar, most probably hosted in microscopic to submicroscopic fluid inclusions, associated with high Cl/K ratios. Infrared laser step-heating experiments on fault vein pseudotachylyte matrices yield strongly discordant age spectra with an overall saddle shape characterised by a minimum at ~ 34 Ma, unrealistically old ages at high temperatures associated with high Cl/K ratios and total gas ages of 41.5–44.3 Ma. Petrographic data and the pronounced compositional similarity between in situ UV laser data on quartz and the high-temperature end member of step-heating analyses suggest that quartz is the main contaminant of the pseudotachylyte age record. In situ laserprobe analyses on pseudotachylyte matrices give concordant ages at ~ 34 Ma for an injection vein and systematically older ages, clustering at $\sim 40-48$ Ma, for fault veins. Although the age cluster fits into the Cenozoic tectonic framework of the region, it is an artefact due to the low spatial resolution of the argon laserprobe compared to the size and spatial distribution of quartz clasts within the pseudotachylyte. The isochron age of 34.11 ± 0.96 Ma, derived from in situ data from the injection vein, overlaps with the

☆ Supplementary data associated with this article can be found in the online version at doi: 10.1016/j.epsl.2004.04.042.

* Corresponding author. Tel.: +39-50-3152270; fax: +39-50-3152360.
E-mail address: g.divincenzo@igg.cnr.it (G. Di Vincenzo).

0012-821X/$ - see front matter
doi:10.1016/j.epsl.2004.04.042

emplacement age of syn-tectonic dykes from nearby areas and is interpreted to date a single episode of coseismic faulting. Regionally, the age of the studied pseudotachylytes represents the first direct onshore evidence of right-lateral strike–slip fault system activity in Victoria Land during the Cenozoic.

Keywords: Ar-40/Ar-39 dating; pseudotachylyte; coseismic faulting; strike–slip fault; northern Victoria Land; Antarctica

1. Introduction

Fault-generated pseudotachylytes typically form in the upper crust [1,2] during high-velocity slip (>0.1 m/s; [3,4]) associated with coseismic faulting [5]. The study of these rock types may therefore provide insight into the activity of ancient faults and allow a better understanding of physical and chemical conditions during earthquake rupturing. Although their origin as products of local cataclasis or melting has been debated in the past (e.g., Wenk [6]), in the last decade, there has been an increasing consensus on a prevalent melt origin. Numerous studies on natural [7–10] or experimentally produced [4,11,12] pseudotachylytes have argued for an origin by frictional melting on the basis of textural criteria and the presence of glass.

Dating pseudotachylytes represents a powerful means to constrain the age of brittle faulting which is otherwise determined indirectly on the basis of stratigraphic constraints and/or by dating syn-tectonic or post-tectonic igneous rocks. Given the generally high K contents in most pseudotachylytes, they are in principle well suited for K–Ar dating (and for the variant ^{40}Ar–^{39}Ar dating). However, due to their peculiar mechanism of formation, pseudotachylytes are strongly heterogeneous: unmelted lithic fragments and mineral clasts from the source rock, frictional glass and neogenic igneous minerals are intimately associated at millimeter to microscopic scales. Complications in ^{40}Ar–^{39}Ar dating of pseudotachylytes may therefore arise due to the coexistence of different reservoirs, each potentially retaining distinct argon isotope signatures: (1) inherited argon (i.e., originated within a mineral relic by decay of ^{40}K prior to the pseudotachylyte-forming event), whose survival may be favoured by the brevity of heating (of the order of a few seconds; [5,13]) during frictional melting; (2) excess argon (i.e., incorporated into the matrix and minerals by processes other than in situ decay); (3) the true radiogenic component (i.e., derived by in situ decay starting from the pseudotachylyte-forming event). Further complications may derive from the presence of alteration phases, which may induce rejuvenation of the matrix age record, and from the low argon-retention properties of silicate glass, which may lead glassy pseudotachylytes to record K–Ar cooling ages rather than formation ages [14].

Despite the importance of and growing interest in fault-generated pseudotachylytes, ^{40}Ar–^{39}Ar studies on these rock types are still limited and the behaviour of K–Ar systematics still needs to be fully clarified. The ^{40}Ar–^{39}Ar method, using both step-heating experiment on bulk samples and/or the in situ laser technique on rock chips, has been applied to pseudotachylytes from different areas with variable success. Step-heating analyses of pseudotachylyte matrices commonly yield very complex age spectra which are difficult to interpret and, less frequently, yield nearly flat age patterns or patterns with a concordant or nearly concordant region [10,15–19]. Although the in situ laserprobe method has proven to be effective in dating some pseudotachylytes [17,20–23], the widely scattered argon ages from pseudotachylyte matrices indicate that the impact of the invariably present mineral clasts on the matrix age record must be carefully evaluated.

This study reports the results of a detailed investigation using ^{40}Ar–^{39}Ar laser experiments in conjunction with mineral and textural analysis of the first record of Cenozoic fault-generated pseudotachylytes in the West Antarctic Rift System of northern Victoria Land. Pseudotachylytes exhibit glassy matrices and were formed at the expense of quartzo-feldspathic metamorphic rocks in the crystalline basement of the Cambro-Ordovician Ross Orogen. The relatively well-constrained geological age of pseudotachylyte formation and the large timespan between the age of the source rock and that of the pseudotachylyte-forming event make these rocks

ideal specimens on which to investigate the effects of mineral clasts on the argon age record of pseudotachylyte matrices. Different gas extraction methods were adopted: infrared (IR) laser step-heating analyses on leached and unleached matrix separates and in situ analyses on rock chips using both IR and ultraviolet (UV) laserprobes.

2. Geological outline and age constraints

The studied pseudotachylytes occur in Palaeozoic stromatic migmatites of the Wilson Terrane [24] high-grade metamorphic complex in northern Victoria Land, which are exposed at the German Gondwana Station on the Ross Sea coast (Fig. 1). Unfaulted migmatites have mesosomes consisting of biotite + quartz + plagioclase ± K-feldspar ± garnet ± cordierite ± muscovite and accessory apatite, zircon, monazite and Fe–Ti oxides [25]. In situ ^{40}Ar–^{39}Ar analyses of fresh migmatites yielded age of 440–460 Ma for both muscovite and biotite (Di Vincenzo, unpublished data). These rocks are affected by brittle faulting at the tip of Priestley Fault (Fig. 1) which is part of an array of major Cenozoic NW–SE striking intraplate right-lateral strike–slip fault systems exposed in northern Victoria Land [26]. The principal zone of displacement in Priestley Fault is characterised by a strong transpressional shear component [27]. Approaching its southern onshore termination, fault splaying broadens the faulted area which is locally nearly 30 km wide. Fault surfaces at Gondwana Station strike WNW–WSE and have dominant right-lateral strike–slip kinematics with subordinate reverse motions [27].

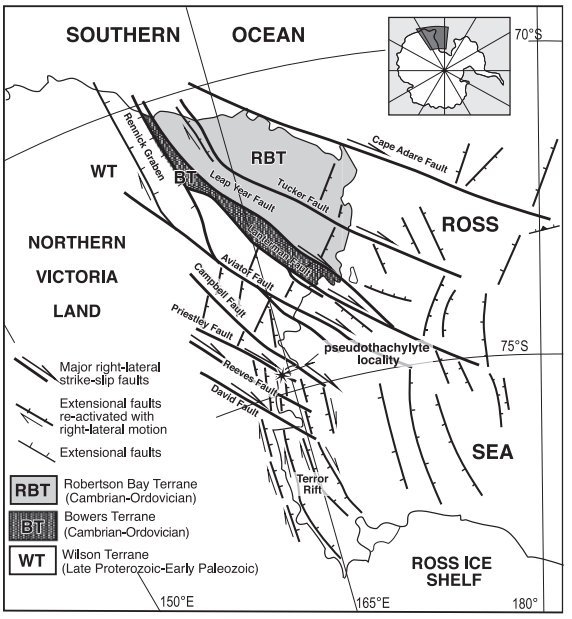

Fig. 1. Tectonic sketch map of Victoria Land (modified after Salvini et al. [26] and Storti et al. [27]).

Important constraints on the age of brittle faulting along the Priestley Fault come from offshore stratigraphic records based on seismic reflection profiles. Transtensional and transpressional deformations along the basin boundary fault system of the western Ross Sea crosscut the RS-U6 unconformity, a major break-up unconformity in the Ross Sea [26]. The age of this unconformity has been constrained to 30–55 Ma [28]. Correlation of the RS-U6 unconformity with the Middle Eocene plate readjustment, which affected the southwest Pacific area [29], yielded an age of ~ 43 Ma. Further constraints come from the geochronological framework of Cenozoic magmatism in northern Victoria Land. Dykes of the Meander Intrusive Group north of Reeves Glacier strike ~ NW–SE and ~ N–S, i.e., parallel to the major right-lateral strike–slip fault systems and to the basin boundary fault system [30]. Field data strongly suggest that dyke emplacement was syn-tectonic [27]. ^{40}Ar–^{39}Ar dating of kaersutite phenocrysts in dykes just north of Priestley Fault yielded indistinguishable Early Oligocene to Middle Eocene ages for the two different dyke occurrences (~ 35.4–45.0 Ma for NW–SE dykes and ~ 34.7–46.7 Ma for N–S dykes; [30]). Finally, apatite fission-track analyses of coastal outcrops in northern Victoria Land [31–33] yielded ages within the 30–40 Ma range and showed long mean track lengths (close to 14 μm), indicating that samples resided for a short time within the partial annealing zone (60–110 °C). These data suggest that coastal outcrops entered the brittle deformation field in the Late Eocene–Early Oligocene and that ambient temperature at the time of pseudotachylyte formation was ≤~ 110 °C. All these data indicate that Priestley Fault certainly developed less than ~ 55 Ma ago and possibly synchronously with the emplacement of syn-tectonic dykes in nearby areas.

3. Experimental procedures

Three samples (F, H and D) were selected for petrographical investigation, microchemical analysis and $^{40}Ar-^{39}Ar$ dating. Petrographical observations were carried out on polished thin sections (derived from the opposite face of the rock chip used for $^{40}Ar-^{39}Ar$ dating), using a light microscope and a Philips XL30 scanning electron microscope (SEM) operating at 20 kV, equipped with an X-ray energy dispersive system. Electron microprobe (EMP) analyses were carried out using a JEOL JX 8600 electron microprobe fitted with four wavelength-dispersive spectrometers, with an accelerating voltage of 15 kV and sample current of 10 nA. Natural standards were used for calibration. The matrix effect was corrected following Bence and Albee [34]. Chlorine was determined under special analytical conditions: the beam spot was defocused to 10 μm to minimise Cl diffusion during analysis, and the counting time and cup current were increased to 100 s and 40 nA, respectively, to improve the detection limit. Cl determinations were retained when above three times the square root of the background level, i.e., about 65 ppm. A total of 18 of 37 determinations overcame this threshold. SEM back-scattered electron (BSE) images of the analysed rock chips were acquired prior to irradiation and after in situ $^{40}Ar-^{39}Ar$ analyses to provide control on the location of the laser pits. The pseudotachylyte matrix of sample H was finely ground in an agate mortar and its X-ray diffraction (XRD) pattern was recorded by a Philips PW1830, operating at 45 kV and 25 mA, using a Cu-anode tube and a sampling width of 0.02°.

Rock chips 8.5 mm in diameter were drilled from double-polished sections (~ 300-μm thick) after removal of the carbon coating and were ultrasonically cleaned in deionised water and methanol. The pseudotachylyte matrices of samples F and H were crushed and sieved, and standard separation techniques were used to concentrate the 160- to 250-μm grain fraction. After the removal of grains containing visible clasts by handpicking under a binocular microscope, the concentrates were cleaned ultrasonically with deionised water and methanol. One aliquot of each sample was leached according to the procedure reported in Koppers et al. [35]. The leaching procedure was used to remove areas affected by secondary alteration which may potentially escape visual inspection of the grains and affect argon data. Samples were wrapped in aluminium foil and were irradiated in the TRIGA reactor at the University of Pavia (Italy) for 20 h along with the biotite standard FCT-3 (27.95 Ma old; [36]). After irradiation, samples were placed in an ultrahigh vacuum laser port and were baked overnight at about 180 °C. In situ laser $^{40}Ar-^{39}Ar$ determinations were carried out using a single-mode laser beam generated by a continuous wave diode-pumped Nd:YAG (Nd-doped yttrium–aluminium–garnet) IR laser (maximum power, 20 W), connected to an external computer-controlled shutter and a pulsed Nd:YAG UV laser (frequency quadrupled and Q-switched). With the purpose of obtaining well-measurable ^{37}Ar and ^{38}Ar beam intensities, the spatial resolution was reduced with respect to the best possible resolution. Each IR determination represents the total gas extracted by several laser shots (5–8 shots, each lasting 12–15 ms at 15 W laser power). The laser shots, each producing a melt pit ~ 100 μm in diameter, were spaced 60 μm apart. The UV-laser, operating at 20 Hz and 0.5–1 mJ per pulse, was focused to ~ 10 μm and was repeatedly rastered by a computer-controlled x–y stage over areas of 0.03–0.06 mm^2 (i.e., ranging from 100×400 to 100×600 μm^2) in order to produce pits ~ 100-μm deep. The sample was observed by a CCD camera coaxial with the laser beam. A total of 15–30 grains of pseudotachylyte–matrix separates (sample mass ~ 0.5–1 mg) and a single grain containing visible clasts from the leached aliquot of sample H were placed in holes 3.0 mm in diameter at the bottom of a copper holder and were incrementally heated by slowly rastering the IR laser defocused to a ~ 2-mm spot size. The IR laser beam was homogenised by a beam-homogeniser lens which produces a flat power distribution. Steps were carried out at increasing laser power to complete melting. After cleanup (10 and 20 min for in situ IR and UV analysis, respectively, and 12 min for IR incremental laser heating analysis), extracted gases were equilibrated via automated valves with a MAP215-50 mass spectrometer fitted with a Balzers SEV217 secondary electron multiplier. Argon isotope peak intensities were measured 10 times for a total of about 20 min. Blanks were analysed every two to four analyses. Data corrected for postirradiation decay, mass discrimination effects, isotopes derived from interfering neutron reactions and blanks are listed in

Tables 2 and 3 in the online version of this paper. Errors are 2σ and do not include the uncertainty in the J value (analytical error) which was included in the total gas ages, the weighted mean ages and in the intercept ages of isochron plots (internal error). The adopted correction factors were: $(^{40}Ar/^{39}Ar)_K = 0.0084$, $(^{38}Ar/^{39}Ar)_K = 0.013$, $(^{36}Ar/^{37}Ar)_{Ca} = 0.00024$ and $(^{39}Ar/^{37}Ar)_{Ca} = 0.00075$. The K/Ca and K/Cl ratios can be derived by multiplying $^{39}Ar_{(K)}/^{37}Ar_{(Ca)}$ and $^{39}Ar_{(K)}/^{38}Ar_{(Cl)}$ by 0.53 and 1.79, respectively.

4. Sample description and petrographical data

Pseudotachylytes developed within cataclasites consisting of plagioclase, quartz, K-feldspar, minor chlorite and very rare white mica. The maximum thickness of pseudotachylyte veins observed in the field is 5–6 cm. Within the selected samples, pseudotachylytes occur as blackish millimetre-thick fault veins a few centimetres long (Fig. 2). Sample H also contains a black to brown millimetre-sized injection vein (Fig. 2d). Note that the rock chip used to separate the matrix of sample H did not contain portions of the injection vein. Pseudotachylytes consist of an isotropic matrix with subangular to rounded clasts of quartz, minor plagioclase and rare K-feldspar. Mineral clasts range from a few microns to several tens of microns in diameter (Fig. 2c,e–g). Mineral clasts in the fault veins represent 20–35 vol.% of the pseudotachylytes; they are less abundant in the injection vein of sample H (9–15 vol.%) where subrounded to rounded mineral clasts are more frequent (Fig. 2f). Pseudotachylytes locally include lithic cataclasite fragments hundreds of microns in diameter (e.g., Fig. 2b). Mineral clasts showing resorption phenomena, pseudotachylyte embayments along the margins of lithic clasts or of the host cataclasite (Fig. 2b) and flow textures, all pointing to a melt origin of the veins (e.g., Magloughlin [7]), are common features in the studied samples. Plagioclase clasts occur as discrete grains within the fault veins while they are strongly resorbed in the injection vein (Fig. 2g). Microlites were rarely observed at the SEM scale in the injection vein of sample H (Fig. 2d). They consist of micron-sized biotite laths and titanite coronae around quartz clasts (Fig. 2g) and, locally, of unresolvable micron- to submicron-sized tablets (probably consisting of plagioclase), disseminated within the pseudotachylyte matrix. Rounded to subrounded cavities a few microns in diameter are frequent and most probably represent vesicles. They are filled by Fe oxides and other darker (under the SEM), unresolvable phases (Fig. 2g). Minor microcracks locally filled with Fe oxides crosscut both the pseudotachylyte veins and host rocks. Quartz, both in the host rock and in the pseudotachylyte clasts, contains numerous tiny (microscopic to submicroscopic) fluid inclusions which give the mineral a turbid appearance. The larger are two-phase (fluid, vapour) inclusions, the smaller are unresolvable.

The XRD pattern (Fig. 3) of pseudotachylyte veins from sample H shows sharp, intense peaks corresponding to quartz reflections, with only a minor presence of feldspars (orthoclase and albite). The pattern also shows a broad "background peak" in the 15°–40° (2θ) range which indicates the presence of glass material [11,12]. The composition of the glassy matrix in the pseudotachylyte fault and in the injection veins is comparable and similar to that of K-feldspar in the source rock (Table 1). However, the pseudotachylyte matrices from both samples have slightly higher Fe and Mg contents with respect to K-feldspar from source rocks. The composition of plagioclase in the source rock ($Ab_{82}An_7Or_{11}$) and pseudotachylyte clasts ($Ab_{89}An_2Or_9$) is comparable. EMP data suggest that the pseudotachylyte matrix was produced by preferential melting of K-feldspar in the source rock. In addition, the different clast/matrix ratios in the fault veins and in the sample H injection vein are probably related to a process of mechanical segregation, such as flow differentiation, rather than to a differential degree of clast resorption. The Cl/K and Ca/K ratios are generally low and less than 0.002 and 0.02, respectively (Table 1).

5. ^{40}Ar–^{39}Ar dating

5.1. Laser step-heating experiments

Pseudotachylyte multigrain fractions show reproducible intrasample and intersample apparent age spectra whose main features can be summarised as follows (Table 2 in the online version of this paper and Fig. 4):

(1) internally discordant age patterns, with an overall (asymmetric) saddle shape;

(2) the minimum of the spectra, which extends for 10–30% of the ^{39}Ar released, occurs at low, comparable temperatures for the four runs and yields lower Ca/K and Cl/K ratios;

(3) the minimum yields comparable apparent ages of 33.3–35 Ma in the four runs;

(4) the majority of steps (representing up to more than 90% of ^{39}Ar released) yield apparent ages

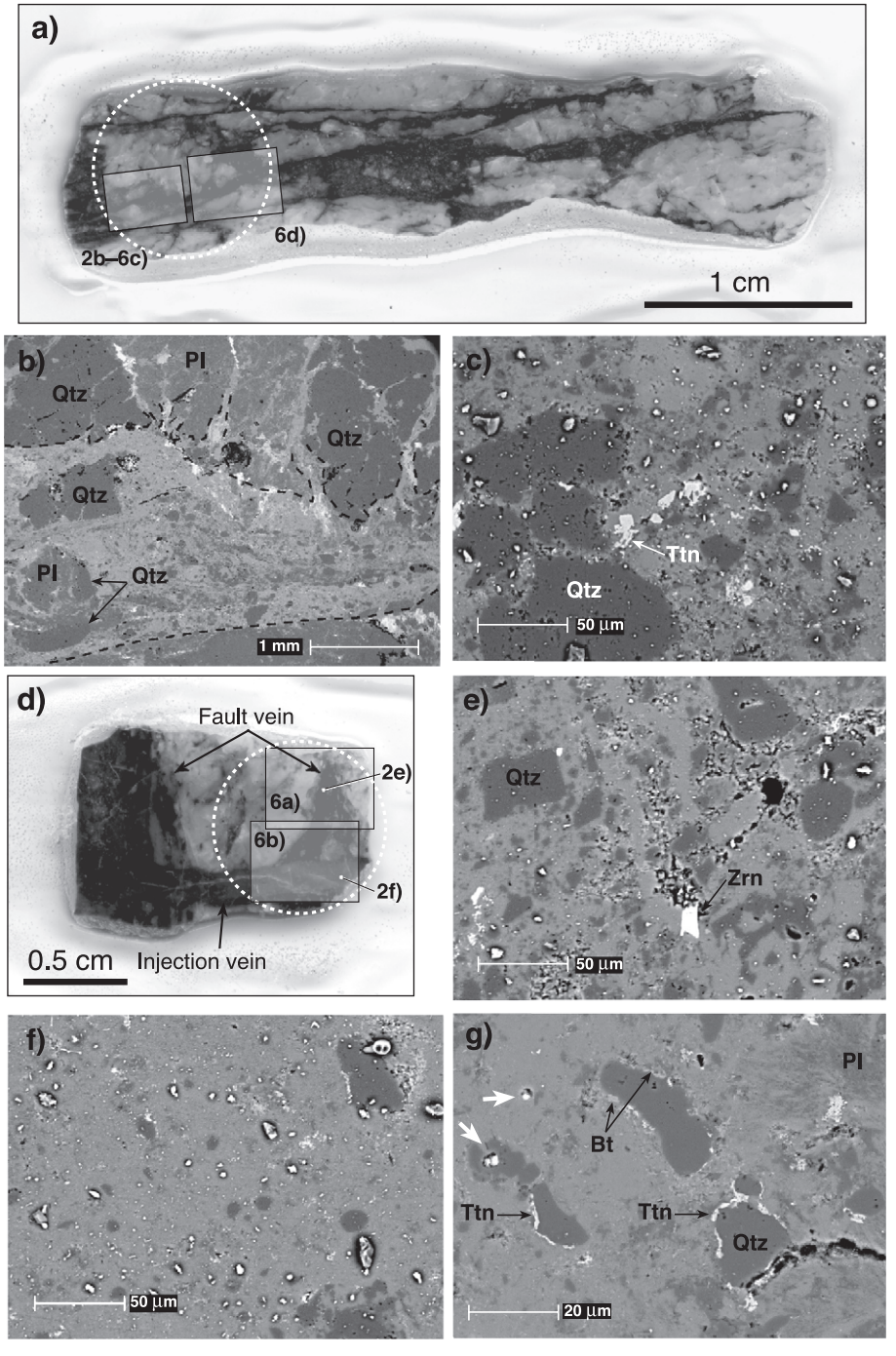

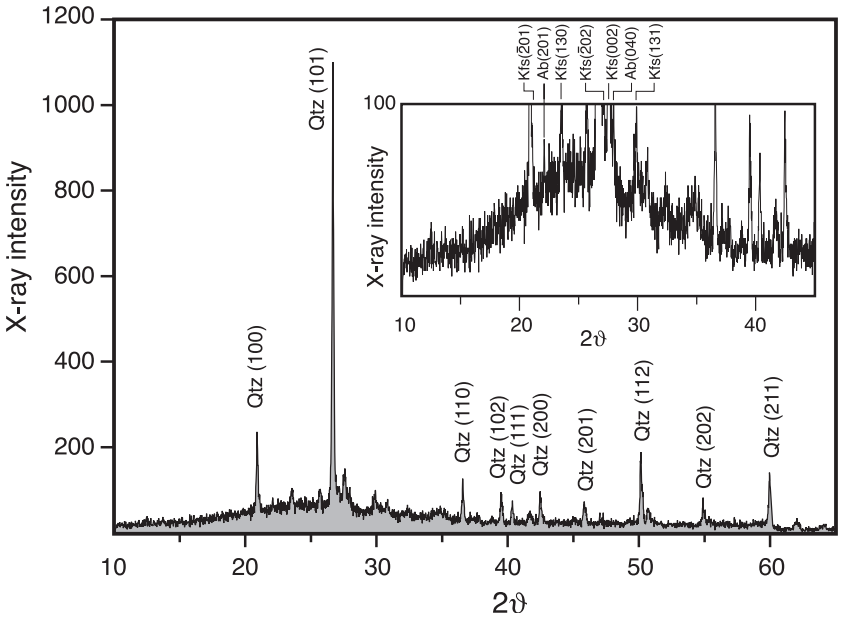

Fig. 3. X-ray diffraction pattern of a pseudotachylyte fault-vein from sample H. Note the broad "background peak" within 15°–40° (2θ) indicating the presence of glass material.

which fall within the 33.3 to 60–70 Ma range; and

(5) apparent ages at high temperatures quickly increase along with Ca/K and Cl/K ratios, and in the final steps, they significantly exceed the age of the Ross Orogen (e.g., up to 2.4 Ga in the leached aliquot of sample H).

The main differences are the higher radiogenic argon contents and lower Cl/K ratios in the low-temperature steps of the leached aliquots than in the unleached ones, suggesting possible removal of minor alteration within microcracks and vesicles by the leaching procedure. Total-gas ages fall within a restricted range (41.46 ± 0.25 to 44.32 ± 0.29 Ma) but do not overlap at 2σ internal error. The release spectrum of the single grain (sample H; Fig. 4) shows general features comparable to those of the multigrain fractions but is characterised by a slightly older total-gas age (45.84 ± 0.41 Ma) and a higher total-gas Ca/K ratio (0.21 vs. ≤0.065 of the multigrain runs), suggesting contamination by a phase with a very high Ca/K ratio. In an $^{36}Ar/^{40}Ar$ versus $^{39}Ar/^{40}Ar$ isochron diagram (Fig. 5), data from laser step-heating experiments define a triangular envelope whose three point mixing end members correspond to: (1) atmospheric argon, (2) an apparent radiogenic argon component about ~ 34 Ma old and (3) an apparent end member with a very high $^{40}Ar/^{36}Ar$ ratio (~ 2000).

5.2. In situ IR and UV laserprobe analyses

The in situ IR spot fusion and UV ablation (rastering mode) techniques were used to investigate intra-

Fig. 2. (a) Photograph of the polished section used for in situ analyses of sample F. The dotted circle indicates the location of the drilled rock chip. (b) Back-scattered electron (BSE) photomicrograph of the area indicated in panel (a). Note the resorption phenomena in quartz and in the lithic fragment (left) and the pseudotachylyte embayments along the margin of the host cataclasite. (c) BSE photomicrograph of a fault vein in sample F (see Fig. 6d for location). (d) Photograph of the polished section used for in situ analyses of sample H. The dotted circle indicates the location of the drilled rock chip. (e) BSE photomicrograph of the fault vein (right) shown in panel (d). Location is also indicated in Fig. 6a. (f) BSE photomicrograph of the injection vein shown in panel (d). Note that the fault vein within the same sample contains many more mineral clasts. (g) BSE photomicrograph of the injection vein with biotite and titanite microlites forming coronae around quartz clasts and a strongly resorbed plagioclase clast; rounded cavities (white arrows) filled by Fe oxides most probably represent vesicles.

Table 1
EMP analyses of pseudotachylyte matrix and K-feldspar from the source rock

Sample	H						F			
	Fault veins		Injection vein		K-feldspar		Fault veins		K-feldspar	
No. of analyses	8		11		6		14		5	
	average	± S.D.	average	± S.D.	average	± S.D.	average	± S.D.	average	± S.D.
SiO_2	65.08	1.30	65.25	1.45	64.32	1.01	64.95	0.94	64.57	1.39
Al_2O_3	19.39	0.49	18.96	0.54	19.41	0.28	19.15	0.42	19.16	0.33
$FeO_{(Total)}$	0.29	0.31	0.42	0.53	0.09	0.11	0.12	0.10	0.03	0.02
MnO	0.03	0.04	0.04	0.02	0.03	0.01	0.04	0.01	0.04	0.03
MgO	0.05	0.06	0.26	0.26	0.03	0.01	0.06	0.04	0.01	0.01
CaO	0.06	0.07	0.09	0.06	0.06	0.03	0.07	0.09	0.07	0.02
Na_2O	0.28	0.09	0.38	0.18	0.44	0.16	0.25	0.09	0.25	0.05
K_2O	15.34	0.66	14.66	0.84	14.90	0.36	15.65	0.40	15.57	0.64
SrO	0.04	0.01	0.10	0.06	0.08	0.03	0.08	0.06	0.10	0.11
BaO	0.13	0.17	0.17	0.03	0.64	0.25	0.25	0.15	0.32	0.36
No. of analyses	7		18		2		5		5	
Cl ppm	< 65–260		< 65–73		< 65–260		< 65–284		< 65–766	
Ca/K	0.0005 –0.0049		< 0.0005 – 0.013		0.011–0.061		< 0.0005 – 0.017		< 0.0006–0.0043	
Cl/K	< 0.0005–0.0020		0.0010–0.0016		0.0008–0.0020		0.0006–0.0021		0.0007–0.0057	

sample and intersample spatial distribution of argon isotopes in pseudotachylyte matrices, in visible clasts enclosed within the pseudotachylytes and in source rock minerals. The UV laser extraction technique was mainly used to sample clasts and minerals in host rocks so as to overcome the difficulty in analysing minerals nearly transparent to the 1064-nm wavelength, e.g., feldspars and quartz [37]. For the purpose of comparison, both IR and UV lasers were used to analyse the pseudotachylytes.

^{40}Ar–^{39}Ar ages from the pseudotachylyte matrix of sample F, even in areas where no clasts were observed during experiments (several tens of microns), span a relatively large interval of 38.2 ± 0.7 to 50.4 ± 1.8 Ma (Table 3 in the online version of this paper and Fig. 6). Younger ages generally have lower Ca/K and Cl/K ratios. Older ages of up to ~ 62 Ma were detected in areas where the pseudotachylyte is visibly clast laden, and ages of up to ~ 380 Ma were found in plagioclase from a lithic cataclasite fragment (Fig. 6c). Argon ages from plagioclase in the host rock vary widely from 60 to 240 Ma. More significantly, quartz from the host rock yields much older ages (up to 2.1 Ga; Table 3 in the online version of this paper and Fig. 6) which exceed the ages of Ross tectono-metamorphic events, suggesting the presence of an excess argon component hosted in quartz. Note that plagioclase and quartz analyses are chemically well distinguishable from those carried out in the pseudotachylyte matrix (Table 3 in the online version of this paper). Plagioclase, in agreement with EMP analyses, exhibits higher Ca/K ratios (up to 0.6), and quartz is characterised by significantly higher Cl/K (up to 0.23) and variably higher Ca/K ratios than those of the pseudotachylyte matrix. In an $^{36}Ar/^{40}Ar$ versus $^{39}Ar/^{40}Ar$ isochron diagram (not shown), argon data from the pseudotachylyte matrix, excluding analyses with the lowest radiogenic argon contents and/or derived from visibly clast-laden areas (analyses 4, 5, 7, 16 and 25, Table 3 in the online version of this paper), define a linear array (MSWD = 1.02) with an intercept age of 31.7 ± 3.5 Ma and an initial $^{40}Ar/^{36}Ar$ ratio of 1528 ± 340 which strikingly compares with quartz $^{40}Ar/^{36}Ar$ ratios (1313 ± 186 to 1845 ± 144) and suggests the presence of trapped nonatmospheric argon.

Results from the sample H fault vein yield a range of ages comparable to that of sample F (Fig. 6a,b), with a slightly younger minimum age (36.3 ± 0.9 Ma). Again, significantly older ages were detected where the pseudotachylyte matrix appears to contain more clasts or within large clasts enclosed in the matrix (Fig. 6). A large (millimetre), ribbon-shaped lithic fragment

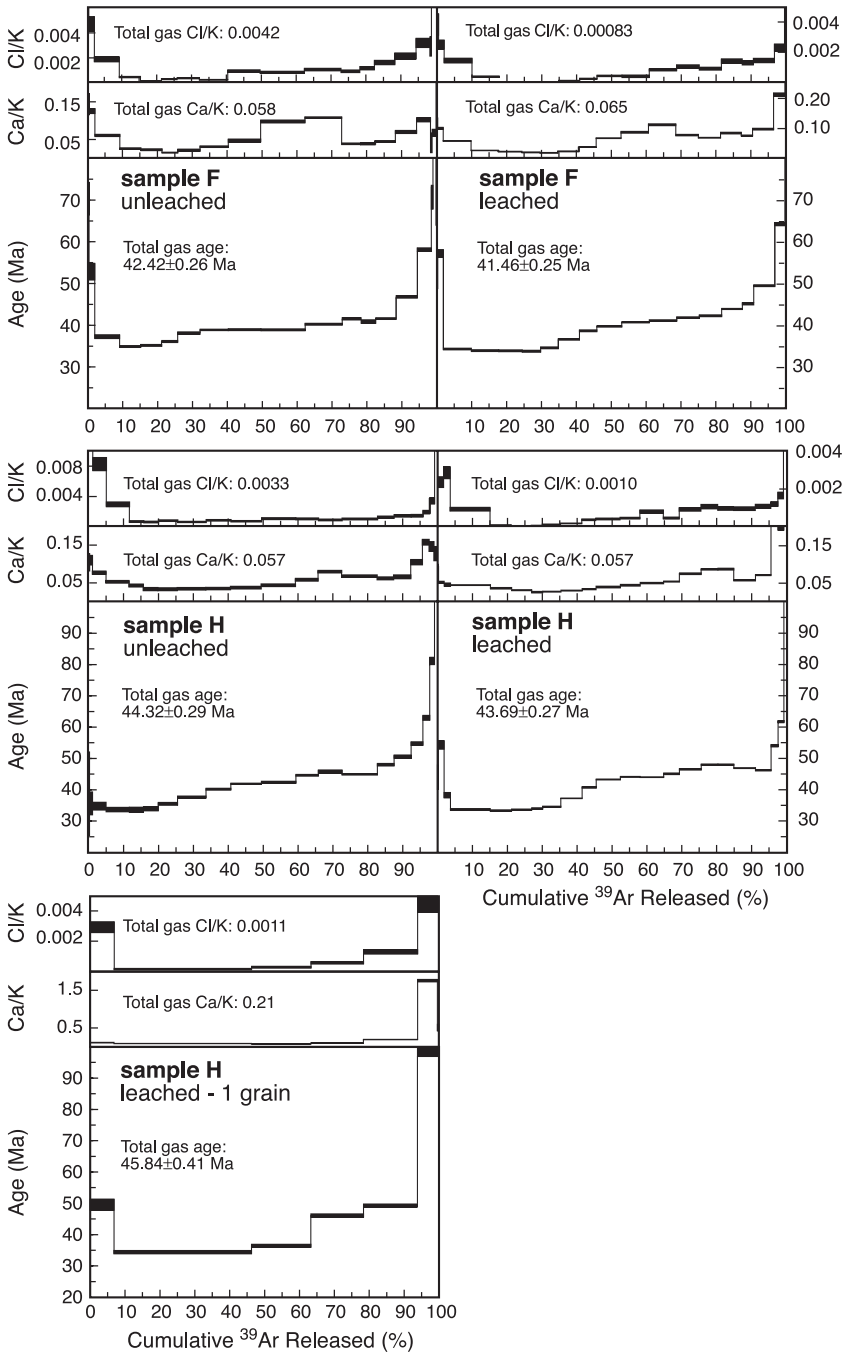

Fig. 4. Age release and Ca/K and Cl/K spectra of pseudotachylyte matrices from samples F and H.

enclosed in the fault vein and mainly consisting of quartz yielded much older ages of up to ~ 700 Ma. Quartz from the host cataclasite again yielded high Cl/K ratios and unrealistically old apparent ages (up to 7.3 ± 1.0 Ga). In contrast, argon data from the injection vein (12 analyses), with the exception of two analyses

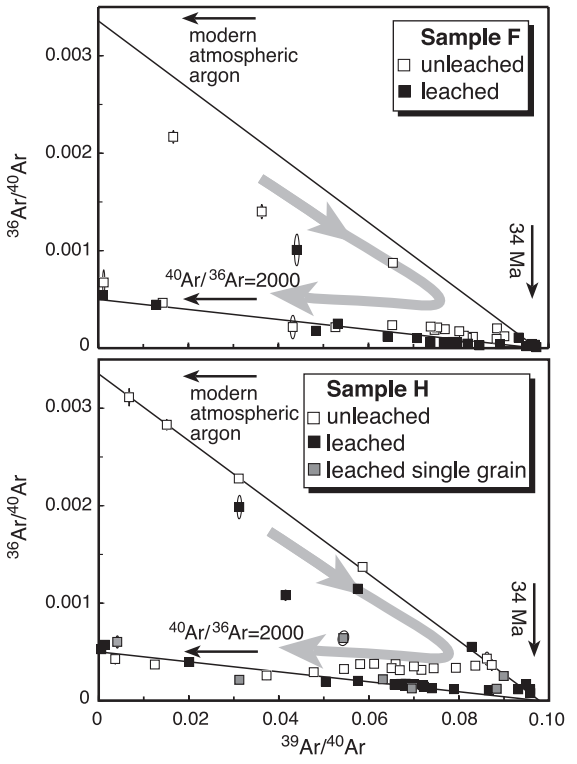

Fig. 5. Isochron plots of data from laser step-heating experiments. The grey arrows describe the trajectory of steps with increasing temperature. Data from samples F (upper) and H (lower) plot within a triangular envelope delimited by three components: (1) modern atmospheric argon ($^{40}Ar/^{36}Ar$ ratio of 295.5), (2) an apparent radiogenic component (~ 34 Ma old), and (3) an apparent component with a very high $^{40}Ar/^{36}Ar$ ratio (~ 2000). Errors are 2σ.

from clast-laden regions close to the contact with the fault vein (analyses 42 and 51; Fig. 6b), yielded ages which overlap at 2σ analytical errors, with a weighted mean date of 34.04 ± 0.37 Ma (MSWD = 1.5). A least-squares fit through these data (MSWD = 1.6) in an $^{36}Ar/^{40}Ar$ versus $^{39}Ar/^{40}Ar$ isochron diagram (not shown) yields an intercept age of 34.11 ± 0.96 and an initial $^{40}Ar/^{36}Ar$ ratio of 292 ± 32, which is indistinguishable from that of modern atmospheric argon (i.e., 295.5), and suggests simple two-component mixing (radiogenic and atmospheric argon).

Sample D was investigated by in situ dating only and yielded ages of ~ 38 to ~ 64 Ma for the pseudotachylyte matrix which lacks visible clasts, of up to ~ 290 Ma for both plagioclase and K-feldspar in the host rock and an age of ~ 3 Ga for quartz. Note that the two K-feldspar analyses from the host rock indicate that K-feldspar is not chemically distinguishable from the pseudotachylyte matrix because it has low Ca/K and Cl/K ratios which fall in the interval detected for the pseudotachylyte matrices.

6. Discussion

6.1. Interpretation of argon data and age of the pseudotachylyte-forming event

Preliminary evaluation of in situ data on the injection vein and fault veins, excluding analyses from visibly clast-laden areas, reveals that more than 90% of the whole data set clusters at 34–50 Ma and more than 70% at 40–50 Ma. In a cumulative frequency diagram (Fig. 7), data from the fault veins show dominant peaks in the 40- to 48-Ma age interval. The remarkable consistency with the expected age for the onset of faulting along the Priestley Fault suggests that the sampled fault rocks record cyclic activity under a high-velocity slip regime. Activity began around 45–48 Ma ago and, as testified by concordant ages of the texturally younger injection vein, ended ~ 34 Ma ago. This inference is consistent with the following observations:

(1) petrographic analysis and the striking intrasample reproducibility of step-heating data on leached and unleached matrix separates suggest that alteration played a negligible role in the studied samples;
(2) the possible cyclic nature of pseudotachylyte generation (occurring not only within a single seismic event but also during diachronic events along the same fault; [3]); and
(3) the expected age interval for the formation of pseudotachylytes deduced from the tectonic framework of the region.

The hypothesis of cyclic slip along the same fault strand, however, strongly contrasts with the following observations which are mainly based on the comparison of in situ data with data from step-heating experiments:

(1) although sample F did not show injection veins texturally comparable to that of sample H, the

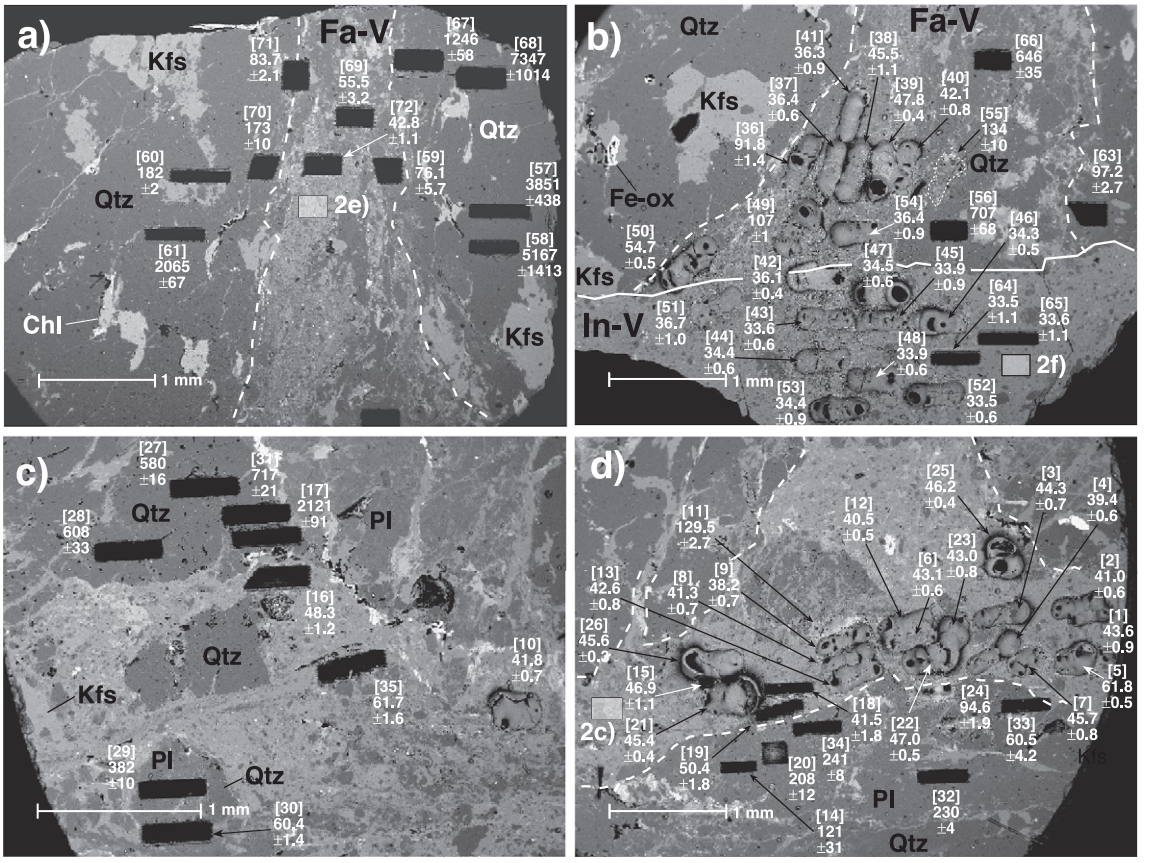

Fig. 6. Back-scattered electron photomicrographs of areas in samples H (a and b) and F (c and d) investigated by argon laser-probe. Errors are 2σ and do not include the uncertainty in the J value. Numbers in brackets correspond to analysis numbers in Table 3 in the online version of this paper; Fa-V, fault vein; In-V, injection vein.

sample F age spectra nevertheless yielded steps as young as 33.5–35 Ma, whereas comparable young ages were not observed by in situ dating;

(2) although the rock chip used to separate the matrix from sample H (in contrast to that used for in situ dating) did not contain a portion of injection vein, the minimum of the saddle in the age profiles still reaches ~ 34 Ma; and

(3) more than 35% of the steps from step-heating experiments yielded ages younger than 40 Ma.

Furthermore, the pronounced isotope disequilibrium detected by in situ dating, even within the same vein (Fig. 6), is well beyond analytical uncertainty. This suggests the primary role of inherited mineral clasts in plaguing argon data and producing an apparently wider age interval.

Petrographic features imaged at the SEM scale suggest that the fine dissemination of clasts within the pseudotachylyte matrix cannot be avoided during $^{40}Ar-^{39}Ar$ laser experiments; neither through detailed examination of grains used for step-heating analysis under the binocular microscope nor by careful selection of target areas during in situ laser analysis. The size of clasts and their distribution within the veins would require a spatial resolution which is well beyond the possibilities of the in situ laserprobe technique. The areas sampled by the laser microprobe and the single grains within the separates inevitably consist of a mixture of pseudotachylyte matrix and

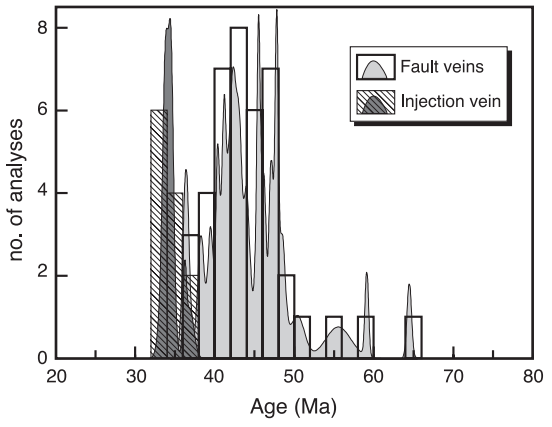

Fig. 7. Histograms of in situ age data from fault veins in samples D, F and H and from the injection vein in sample H. The cumulative probability distribution was calculated by the Isoplot/Ex program v. 2.3 [47], using 2σ analytical uncertainty.

mineral clasts, as confirmed by step-heating experiments. Indeed, all five runs yielded discordant age spectra, with high-temperature ages significantly exceeding the permissible time interval, and age-step variations correlated with variations in elemental ratios derived from argon isotopes (i.e., Ca/K and Cl/K). The strong intrasample and intersample consistency of data obtained through different extraction techniques (step-heating and in situ) suggests that loss and/or redistribution by recoil during sample irradiation of neutron-produced $^{39}Ar_K$, $^{38}Ar_{Cl}$, $^{37}Ar_{Ca}$ (see also Magloughlin et al. [17]) played an insignificant role in the studied samples. Accordingly, we should conclude that step-heating analyses yield information on chemically distinct reservoirs with different argon isotope signatures. This hypothesis is strongly supported by the striking consistency of in situ data derived from large clasts and from the host rock with the argon isotope signature of the high-temperature steps of incremental heating experiments. The implication of the above finding is that matrix separates are contaminated by clasts to some extent. Because the five runs have total-gas ages which fall just within the 40–50 Ma interval, we must conclude that even the clustering of in situ ages from the fault veins at 40–50 Ma is plagued by the presence of clasts.

Petrographic data indicate that the main possible reservoirs of argon isotopes within the pseudotachylyte veins are the glassy matrix (compositionally resembling K-feldspar) and host-derived quartz, plagioclase and K-feldspar. Among clasts, quartz is by far the most abundant constituent, whereas feldspars are volumetrically subordinate. In situ analyses on both large clasts within the fault veins and minerals from the host rock indicate that quartz and feldspars contain extraneous argon (either inherited or excess argon), with the implication that the pseudotachylyte-forming event did not totally reset the isotope signature of minerals from the source, found in the host rock adjacent to the vein margins or as clasts within the veins (cf. [17,18,20,23]). Feldspars yielded argon ages that never exceed the age of Ross tectonometamorphic events, suggesting that they contain a partially reset inherited-argon component. In contrast, quartz gave unrealistically old ages, even older than the Earth, which are associated with very high Cl/K ratios and which unequivocally indicate the presence of trapped excess argon. Taking into account the volume sampled by the UV laser during in situ experiments and normalising argon data to the expected age for pseudotachylyte formation, quartz is found to contain approximately 10–50 ppb of ^{40}Ar (extremes of 5 and 180 ppb). In light of the radiogenic argon production rate of only 1 ppb/Myear in a system with a K-feldspar-like potassium content, concentrations of 10–50 ppb cannot be considered negligible. A mixture composed of a phase compositionally similar to K-feldspar with an argon age of ~34 Ma and quartz containing 10–50 ppb of parentless ^{40}Ar yields ages of ~37–47 Ma and 39–61 Ma for the proportions (based on petrographic investigation) 80:20 and 65:35, respectively. Therefore, contamination by quartz clasts alone can account for the experimentally observed clustering of ages from fault veins at 40–50 Ma, again suggesting that such a clustering is unreliable. This interpretation is broadly consistent with in situ analyses of the sample F fault vein; in an isochron diagram data yield a well-defined linear array, with an intercept age overlapping within error the ~34-Ma age of the injection vein and with a $^{40}Ar/^{36}Ar$ ratio similar to the argon isotope signature directly determined for quartz. The role of feldspars is more difficult to quantify. However, examination of data from incremental heating analysis in three-isotope correlation diagrams ($^{40}Ar^*/^{39}Ar_K$ vs. $^{37}Ar_{Ca}/^{39}Ar_K$ and $^{40}Ar^*/^{39}Ar_K$ vs. $^{38}Ar_{Cl}/^{39}Ar_K$) converted to age and elemental Ca/K and Cl/K ratios (see Villa

[38]), and the compositions of minerals from the host rock as defined by in situ argon analysis (Fig. 8) suggest that plagioclase was probably involved in the intermediate- to high-temperature steps. Note that in the age vs. Ca/K diagram, data from in situ analysis on pseudotachylyte matrices and those from step-heating experiments plot within divergent mixing trends which point to quartz and plagioclase compositions. Divergent mixing trends were also reported by Müller et al. [18] in fault-generated pseudotachylytes related to the Insubric Fault System of the Alps, and in most cases, these trends were attributed to alteration and clast phases.

The ability of quartz to accommodate significant amounts of argon has been demonstrated both experimentally [39,40] and based on the study of natural examples [41,42]. Natural examples reveal a close correlation between the amount of excess argon and that of chlorine (determined by neutron-produced $^{38}Ar_{Cl}$), suggesting that excess argon resides in saline fluid inclusions (e.g., Kelley et al. [41] and Cumbest et al. [43]). The Cl–excess argon relationship in our samples is shown by the well-defined positive correlation between age and Cl/K ratios for the whole data set (Fig. 8). The correlation, however, becomes more scattered and less defined towards lower Cl/K ratios and younger ages (i.e., approaching the matrix end-member), most probably due to submillimeter-scale chemical heterogeneity within the pseudotachylyte matrix, as revealed by EMP data and found in other natural pseudotachylytes [18,44]. This strongly hampers the identification of the age of pure pseudotachylyte matrix from three-isotope plots.

Other works (e.g., Sherlock and Hetzel [23] and Müller et al. [18]) also have hypothesised that quartz and plagioclase clasts can have a profound effect on the argon isotope signature of pseudotachylyte matrices. Our results provide compelling evidence that this is the case. Quartz is by far the predominant mineral clast within most natural pseudotachylytes of the continental crust. When quartz clasts are documented by petrographic investigation, their role in plaguing argon data should be carefully assessed. Contamination by clast-hosted extraneous argon due to fine dissemination of clasts within pseudotachylyte matrices may produce clustering of in situ argon ages, and such contamination is not necessarily revealed by distribution of data in isochron plots (e.g., data from sample D or from sample H fault vein). Furthermore, the use of the in situ laserprobe technique at the highest spatial resolution with the aim of resolving sample heterogeneity represents a potential pitfall, especially for young pseudotachylytes. Analysis carried out on very small samples yields argon data affected by large errors, possibly obscuring heterogeneity and decreasing the precision of chemical information derived from reactor-produced argon isotopes (K, Cl and Ca). This could make contamination by clast-hosted extraneous argon much more cryptic and difficult to identify. Examination of step-heating profiles reveals that the excess argon–chlorine signature is only clearly revealed at high temperatures. However, as discussed in other studies [41,43], decrepitation of fluid inclusions is not only a function of P–T conditions during trapping but also of the strength of the host mineral and the size of inclusions [45]. This means that very small inclusions (micron- to submicron-sized in diameter) may withstand very high temperatures. This interpretation is broadly compatible with the release spectra for quartz reported in other studies [38,39]. We therefore attribute the staircase segment after the minimum in the step-heating age spectra to a sequence of increasing fluid inclusion decrepitation temperatures coupled with involvement of plagioclase, as indicated by the data distribution in three-isotope correlation plots. We believe that only an integrated approach, which involves chemical and textural characterisation at the microscale and fully exploits the complementarity of ^{40}Ar–^{39}Ar step-heating and in situ methods, has the full potential to disentangle the complexity of pseudotachylyte rocks (cf. [17,18]).

We conclude that, despite the good fit with the Cenozoic tectonic framework of the region, the clustering of ages from the fault veins at 40–50 Ma is meaningless; it is an artefact due to the low spatial resolution of the in situ laser method compared to the size and spatial distribution of mineral clasts within the pseudotachylyte matrix. With the exception of some analyses from areas visibly rich in clasts or containing large clasts, the sampled areas within the fault veins correspond to matrix–clast mixtures with nearly constant proportions. We instead consider reliable the age of $\sim$ 34 Ma derived from the injection vein of sample H and the isochron age of 34.11 ± 0.96 Ma a conservative estimates for the argon age of

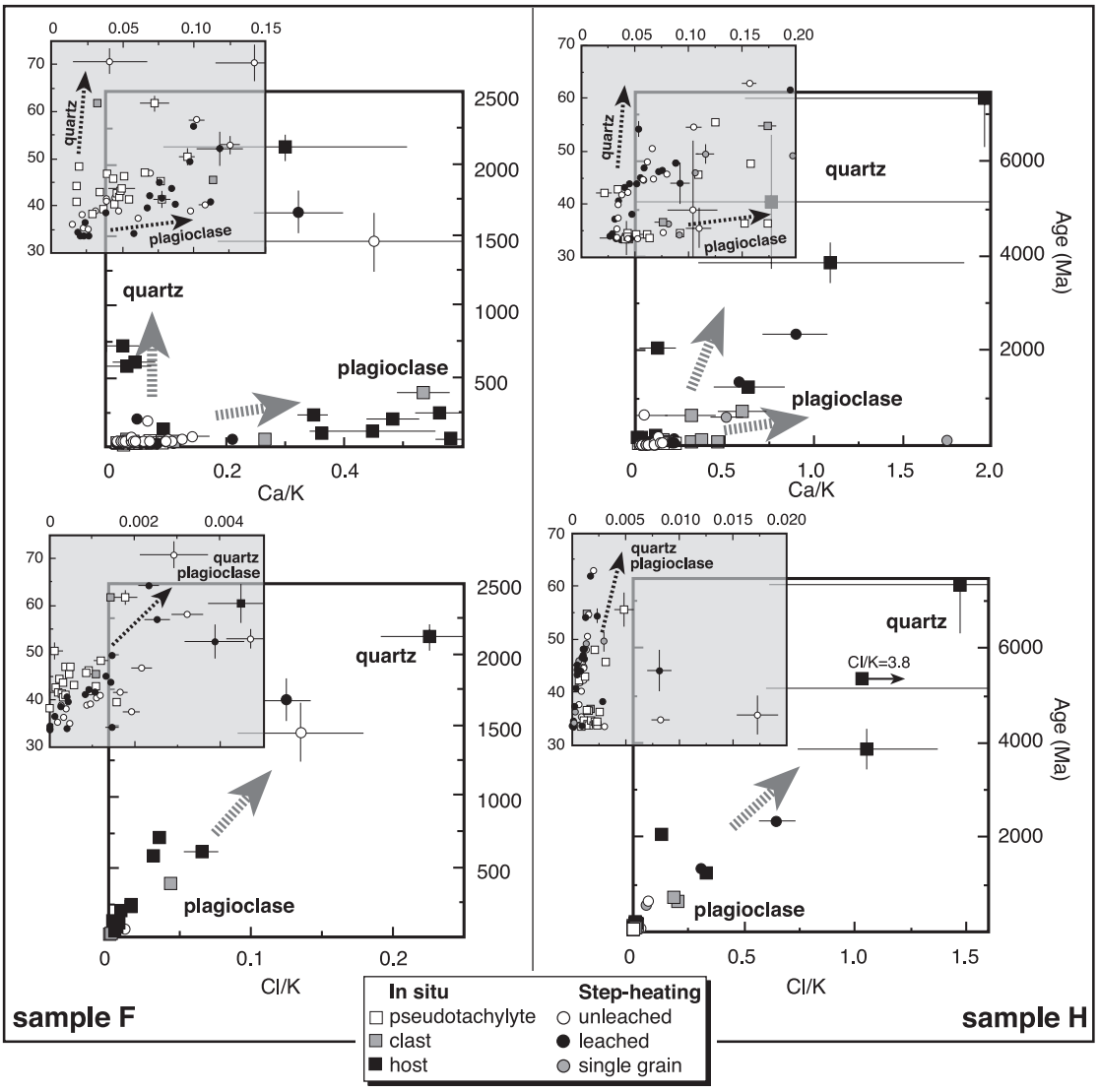

Fig. 8. Three-isotope correlation plots converted to age and elemental Ca/K (upper) and Cl/K (lower) ratios for data from step-heating and in situ experiments on samples F (left) and H (right). Errors are 2σ.

glassy matrices formed during a major episode of coseismic faulting. The strong intrasample and intersample consistency of argon data, and the agreement of the argon age from the pseudotachylyte matrix with the age of emplacement of syn-tectonic dykes from nearby areas, suggests that argon loss after solidification of pseudotachylytes was negligible and that the ~ 34-Ma age most likely dates the time of pseudotachylyte formation.

6.2. Regional significance of pseudotachylyte age

The Cenozoic to present tectonic framework of northern Victoria Land is dominated by an array of right-lateral fault systems [26] which are considered responsible for the generation and emplacement of Cenozoic magmas [26,30]. However, to date, the age of fault system activity has mainly been inferred from the interpretation of seismic reflection lines.

Additionally, indirect evidence for Middle to Late Eocene fault activity has been recently derived from apatite fission-track thermochronology in the northern segment of the Lanterman Fault close to the Southern Ocean coast (Fig. 1; [46]). The age of the Priestley pseudotachylyte provides the first direct evidence of Cenozoic strike–slip tectonics in Victoria Land. It also confirms the hypothesis that right-lateral seismogenic faulting occurred concurrently with emplacement of mafic dykes in the region. Furthermore, the closeness of age between the Priestley Fault pseudotachylyte on the Ross Sea and movement at the Southern Ocean-end of the Lanterman Fault attests to the dynamic connection between the Ross Sea and Southern Ocean during the Cenozoic.

Acknowledgements

G. Giorgetti is acknowledged for support during SEM investigation and P. Orlandi for access to the XRD facility. We are grateful to C.M. Hall and J.G. Spray for their constructive reviews. The argon laserprobe facility was funded by Programma Nazionale di Ricerche in Antartide (PNRA). Research was funded by CNR and PNRA. *[SK]*

References

[1] R.H. Maddock, J. Grocot, M. van Nes, Vesicles, amygdales and similar structures in fault-generated pseudotachylytes, Tectonophysics 20 (1987) 419–432.
[2] A.M. Killick, C. Roering, An estimate of the physical conditions of pseudotachylyte formation in the West Rand Goldfield, Witwatersrand Basin, South Africa, Tectonophysics 284 (1998) 247–259.
[3] J.G. Spray, A physical basis for the frictional melting of some rock-forming minerals, Tectonophysics 204 (1992) 205–221.
[4] J.G. Spray, Pseudotachylyte controversy: fact or friction? Geology 23 (1995) 1119–1122.
[5] R.H. Sibson, Generation of pseudotachylyte by ancient seismic faulting, Geophys. J. R. Astron. Soc. 43 (1975) 775–794.
[6] H.-R. Wenk, Are pseudotachylytes products of fracture or fusion? Geology 6 (1978) 507–511.
[7] J.F. Magloughlin, Microstructural and chemical changes associated with cataclasis and frictional melting at shallow crustal levels: the cataclasite–pseudotachylyte connection, Tectonophysics 204 (1992) 243–260.
[8] T. Shimamoto, H. Nagahama, An argument against a crush origin for pseudotachylytes based on analyses of clast-size distribution, J. Struct. Geol. 14 (1992) 999–1006.
[9] A. Camacho, R.H. Vernon, J.D. Fitz Gerald, Large volumes of anhydrous pseudotachylyte in the Woodroffe Thrust, eastern Musgrave Ranges, Australia, J. Struct. Geol. 17 (1995) 371–383.
[10] N.R. Warr, B.A. van der Pluijm, D.R. Peacor, C.M. Hall, Frictional melt pulse during ~1.1 Ma earthquake along the Alpine Fault, New Zealand, Earth Planet. Sci. Lett. 209 (2003) 39–52.
[11] A. Lin, T. Shimamoto, Selective melting processes as inferred from experimentally generated pseudotachylyte, J. Asian Earth Sci. 16 (1998) 1–13.
[12] A. Tsutsumi, Size distribution of clasts in experimentally produced pseudotachylytes, J. Struct. Geol. 21 (1999) 305–312.
[13] M.T. Swanson, Fault structure, wear mechanisms and rupture processes in pseudotachylyte generation, Tectonophysics 204 (1992) 223–242.
[14] G.B. Hazelton, G. Axen, O. Lovera, Argon retention properties of silicate glasses and implications for $^{40}Ar/^{39}Ar$ age and noble gas diffusion studies, Contrib. Mineral. Petrol. 145 (2003) 1–14.
[15] W.U. Reimold, E.K. Jessberger, T. Stephan, $^{40}Ar–^{39}Ar$ dating of pseudotachylyte from the Vredefort dome, South Africa: a progress report, Tectonophysics 171 (1990) 139–152.
[16] H.R. Wenk, L.R. Johnson, L. Ratschbacher, Pseudotachylytes in the eastern peninsular ranges of California, Tectonophysics 321 (2000) 253–277.
[17] J.F. Magloughlin, C.M. Hall, B.A. van der Pluijm, $^{40}Ar–^{39}Ar$ geochronometry of pseudotachylytes by vacuum encapsulation: North Cascade Mountains, Washington, USA, Geology 29 (2001) 51–54.
[18] W. Müller, S.P. Kelley, I.M. Villa, Dating fault-generated pseudotachylytes: comparison of $^{40}Ar/^{39}Ar$ stepwise-heating, laser-ablation and Rb–Sr microsampling analyses, Contrib. Mineral. Petrol. 144 (2002) 57–77.
[19] C. Davidson, K.J. Davis, M.B. Christopher, C.H. Tape, J. Singleton, B. Singer, Age, origin, and significance of brittle faulting and pseudotachylyte along the Coast Shear Zone, Prince Rupert, British Columbia, Geology 31 (2003) 43–46.
[20] S.P. Kelley, S.M. Reddy, R. Maddock, Laser-probe $^{40}Ar/^{39}Ar$ investigation of a pseudotachylyte and its host rock from the Outer Isle thrust, Scotland, Geology 22 (1994) 443–446.
[21] J.G. Spray, S.P. Kelley, W.U. Reimold, Laser probe argon-40/argon-39 dating of coesite- and stishovite-bearing pseudotachylytes and the Vredefort impact event, Meteoritics 30 (1995) 335–343.
[22] J.A. Karson, C.K. Brooks, M. Storey, M.S. Pringle, Tertiary faulting and pseudotachylytes in the East Greenland volcanic rifted margin: seismogenic faulting during magmatic construction, Geology 26 (1998) 39–42.
[23] S. Sherlock, R. Hetzel, A laser-probe $^{40}Ar/^{39}Ar$ study of pseudotachylyte from the Tambach fault Zone, Kenya: direct isotopic dating of brittle faults, J. Struct. Geol. 23 (2001) 33–44.
[24] J.D. Bradshaw, M.G. Laird, The pre Beacon geology of north-

ern Victoria Land: a review, in: R.L. Oliver, P.R. James, J.B. Jago (Eds.), Antarctic Earth Science, Australian Academy of Sciences, Canberra, 1983, pp. 98–101.
[25] R. Palmeri, P–T paths and migmatite formation: an example from Deep Freeze Range, northern Victoria Land, Antarctica, Lithos 42 (1997) 47–66.
[26] F. Salvini, G. Brancolini, M. Busetti, F. Storti, F. Mazzarini, F. Coren, Cenozoic geodynamics of the Ross Sea Region, Antarctica: crustal extension, intraplate strike–slip faulting and tectonic inheritance, J. Geophys. Res. 102 (1997) 24669–24696.
[27] F. Storti, F. Rossetti, F. Salvini, Structural architecture and displacement accommodation mechanisms at the termination of the Priestley Fault, northern Victoria Land, Antarctica, Tectonophysics 341 (2001) 141–161.
[28] M. Busetti, A new constraint for the age of Unconformity U6 in the Ross Sea, Terra Antart. 1 (1994) 523–526.
[29] J.J. Veevers, Change of tectono-stratigraphic regime in the Australian plate during the 99 Ma (mid-Cretaceous) and 43 Ma (mid-Eocene) swerves of the Pacific, Geology 28 (2000) 47–50.
[30] S. Rocchi, P. Armienti, M. D'Orazio, S. Tonarini, J.R. Wijbrans, G. Di Vincenzo, Cenozoic magmatism in the western Ross Embayments: role of mantle plume versus plate dynamics in the development of the West Antarctic Rift System, J. Geophys. Res. 107 (B9) (2002) 2195–2217.
[31] M.L. Balestrieri, G. Bigazzi, New apatite fission-track data from a region south of Terranova Bay in the southern part of northern Victoria Land, Antarctica, Geophys. Res. Abstr. 5 (2003) 03879.
[32] M.L. Balestrieri, G. Bigazzi, C. Ghezzo, Uplift-denudation of the Transantarctic Mountains between the David and the Mariner Glaciers, northern Victoria Land (Antarctica): constraints by apatite fission-track analysis, in: C.A. Ricci (Ed.), The Antarctic Region: Geological Evolution and Processes, Terra Antartica Pub., Siena, 1997, pp. 547–554.
[33] M.L. Balestrieri, G. Bigazzi, C. Ghezzo, B. Lombardo, Fission track dating of apatites from Granite Harbour Intrusive suite and uplift-denudation history of the Transantarctic Mountains in the area between the Mariner and David Glaciers (northern Victoria Land (Antarctica), Terra Antart. 1 (1994) 82–87.
[34] A.E. Bence, A.L. Albee, Empirical correction factors for the electron microanalysis of silicates, oxides, carbonates, phosphates and sulphates, Ann. Chem. 42 (1968) 1408–1414.
[35] A.A.P. Koppers, H. Staudigel, J.R. Wijbrans, Dating crystalline groundmass separates of altered Cretaceous seamount basalts by the $^{40}Ar/^{39}Ar$ incremental heating technique, Chem. Geol. 166 (2000) 139–158.
[36] A.K. Baksi, D.A. Archimbald, E. Farrar, Intercalibration of $^{40}Ar/^{39}Ar$ dating standards, Chem. Geol. 129 (1996) 307–324.
[37] S.P. Kelley, N.O. Arnaud, S.P. Turner, High spatial resolution $^{40}Ar/^{39}Ar$ investigations using an ultraviolet laser probe extraction technique, Geochim. Cosmochim. Acta 58 (1994) 3519–3525.
[38] I.M. Villa, Radiogenic isotopes in fluid inclusions, Lithos 55 (2001) 115–124.
[39] K. Roselieb, P. Blanc, H. Büttner, A. Jambon, W. Rammensee, M. Rosenhauer, D. Vielzeuf, H. Walter, Experimental study of sorption in quartz: evidence for argon incompatibility, Geochim. Cosmochim. Acta 61 (1997) 533–542.
[40] E.B. Watson, D.J. Cherniak, Lattice diffusion of Ar in quartz, with constraints of Ar solubility and evidence of nanopores, Geochim. Cosmochim. Acta 67 (2003) 2043–2062.
[41] S.P. Kelley, G. Turner, A.W. Butterfield, T.J. Shepherd, The source and significance of argon isotopes in fluid inclusions from areas of mineralization, Earth Planet. Sci. Lett. 79 (1986) 303–318.
[42] D. Vance, M. Ayres, S.P. Kelley, N. Harris, The thermal response of a metamorphic belt to extension: constraints from laser Ar data on metamorphic micas, Earth Planet. Sci. Lett. 162 (1998) 153–164.
[43] R.J. Cumbest, E.L. Johnson, T.C. Onstott, Argon composition of metamorphic fluids: implications for $^{40}Ar/^{39}Ar$ geochronology, Geol. Soc. Amer. Bull. 106 (1994) 942–951.
[44] S.P. Kelley, J.G. Spray, A Late Triassic age for the Rochechouart impact structure, France Meteor. Planet. Sci. 32 (1997) 629–636.
[45] E. Roedder, Fluid inclusions. Review in Mineralogy, vol. 12, Mineral. Soc. Am., 1984, 644 pp.
[46] F. Rossetti, F. Lisker, F. Storti, A.L. Läufer, Tectonic and denudational history of the Rennick Graben (northern Victoria Land): implications for the evolution of rifting between East and West Antarctica, Tectonics 22 (2003) doi:10.1029/2002TC001416.
[47] K.R. Ludwig, User's manual for Isoplot/Ex version 2.3, a geochronological toolkit for Microsoft Excel, Berkeley Geochronology Center Special Publication 1a (2000) 54.